



Reduced Pressure Effect on Smoke Layer Plug-Holing Behavior of Tunnel Fires with a Naturally Ventilated Vertical Shaft

Jie Wang *, Yanlong Song, Yongjie Fan and Xuepeng Jiang, School of Resource and Environmental Engineering, Wuhan University of Science and Technology, 947 Heping Avenue, Qingshan District, Wuhan 430081 Hubei, China, Hubei Research Center of Industrial Safety Engineering Technology, Wuhan 430081 Hubei, China; Fire Safety Technology Institute, Wuhan University of Science and Technology, Wuhan 430081 Hubei, China
Kaihua Lu, Faculty of Engineering, China University of Geosciences (Wuhan), Wuhan 430074 Hubei, China

Received: 29 November 2022/**Accepted:** 19 September 2023/**Published online:** 30 October 2023

Abstract. The fire smoke exhaust behavior of tunnels with naturally ventilated vertical shafts at high altitude area is different from that at standard atmospheric pressure due to the unconventional fire smoke transportation at reduced pressure. Smoke layer plug-holing is an unfavorable phenomenon for the smoke exhaust efficiency of tunnels with vertical shafts. Therefore, theoretical analysis and numerical simulation of the smoke layer plug-holing behavior of the naturally ventilated vertical shafts at ambient pressure of 60 kPa, 70 kPa, 80 kPa, 90 kPa and 101 kPa were conducted. Since the flame height for tunnel fires with the same heat release rate increases at reduced pressure, the smoke temperature and flow velocity beneath the ceiling are enlarged, which increases the horizontal inertia force of smoke beneath the bottom of the shaft to cause high smoke temperatures and violent smoke diffusion within the shaft, and then the degree of smoke layer plug-holing is weakened. The critical Richardson number (Ri) for predicting the occurrence of plug-holing falls to 1.08 at 60 kPa and has a non-linear relationship to the pressure coefficient. Similarly, the plug-holing height decreases with the decrease in ambient pressure, and a global correlation for the plug-holing height that is positive to the 1.77 power of the Richardson number is proposed based on the theoretical analysis and simulated results.

Keywords: Reduced pressure, Vertical shaft, Plug-holing, Richardson number, Plug-holing height

Abbreviations

A_{1-4}	Fitting coefficient
A_{shaft}	Vertical shaft cross-sectional area (m^2)
C_p	Specific heat of air (J/kg·K)
D^*	Characteristic diameter
d	Smoke layer thickness below the shaft opening (m)

* Correspondence should be addressed to: Jie Wang, E-mail: wangjie87@wust.edu.cn



d_g	Grid size (m)
F_h	Horizontal inertia force (N)
F_v	Vertical buoyancy force (N)
g	Gravitational acceleration (m^2/s)
H	Hydraulic tunnel height defined as the ratio of 4 times the tunnel cross-sectional area to the tunnel perimeter (m)
h^*	Dimensionless shaft height
h	Shaft height (m)
h_c	Heat of combustion (kJ/kg)
h_p^*	Dimensionless plug-holing height
h_p	Plug-holing height (m)
h_{shaft}	Shaft height (m)
k_{1-7}	Fitting coefficient
l_{shaft}	Shaft length (m)
M	Molar mass of air (g/mol)
\dot{m}	Burning rate (kg/s)
n	Amount of gas substance
P	Pressure of ideal gas (kPa)
p	Ambient pressure (kPa)
p_x	Reduced pressure of x kPa (kPa)
p_{std}	Standard atmospheric pressure (kPa)
Q_c	Convective heat release rate (kW)
Q^*	Dimensionless heat release rate
R	Ideal gas constants
Ri'	Richardson number
Ri^*	Richardson number defined by Zhao et al.'s study
Ri_x	Richardson number at the reduced pressure of x kPa
T	Thermodynamic temperature of ideal gas (K)
T_a	Ambient temperature (K)
T_s	Smoke temperature below the shaft (K)
ΔT_s	Smoke temperature rising below the shaft (K)
V	Volume of ideal gas (m^3)
v	Horizontal flow rate of the smoke below the shaft (m/s)
w	Width of the tunnel (m)
w_s	Width of the shaft (m)
x	Longitudinal position from the fire source (m)

Greek symbols

α	Pressure coefficient
$\Delta\rho$	Density difference between smoke and ambient air (kg/m^3)
ρ	Smoke density (kg/m^3)
ρ_{air}	Air density (kg/m^3)
ρ_{s0}	Density of smoke without smoke exhaust (kg/m^3)

1. Introduction

Recently, many high-altitude tunnels have emerged the world, such as the Yankou mountain tunnel in China and the Eisenhower-Johnson Memorial tunnel in the United States. Smoke is the most fatal factor for the tunnel construction and the trapped people [1]. Vertical shafts as a natural smoke extraction mode are widely used in tunnels due to their economy and environmental protection [2]. For exam-

ple, the high-altitude Kunming metro system using vertical shafts has achieved great operational and economic benefits. Meanwhile reduced pressure which alters fire smoke transportation brings a major challenge to the naturally ventilated vertical shaft design of high-altitude tunnels [3].

Considerable research has been conducted on tunnel fires with naturally ventilated vertical shafts, and mainly focuses on the fire smoke characteristics (Li et al. [4], Tang et al. [5], and Ren et al. [6], etc.), smoke exhaust efficiency and optimization (Kashef et al. [7], Yi et al. [8], and Ji et al. [9], etc.), tunnel fire evacuation (Cano-Moreno et al. [10], Chen et al. [11], Krol et al. [12]), smoke back-layering length (Li et al. [13], Zhang et al. [14], Zhang et al. [15], etc.), and influence factors for smoke layer plug-holing (Zhao et al. [16], Liu et al. [17], Liu et al. [18], etc.). In the aspect of smoke layer plug-holing behavior in tunnel shafts which has a significant impact on the smoke extraction efficiency, Ji et al. [19] firstly revealed two special phenomena (plug-holing and boundary layer separation) and proposed a critical plug-holing judging criterion (i.e., a new Richardson number Ri'). Then, some researchers [20, 21] verified the applicability of the critical plug-holing criterion under different conditions. For example, Jiang et al. [20] conducted a series of tunnel fire experiments on smoke exhaust under the vertical shaft and longitudinal ventilation, which showed that the critical plug-holing criterion $Ri' = 1.4$ was still applicable. The smoke exhaust characteristics of shafts arranged in the middle and above the sides of the tunnel were also studied by Jiang et al. [21], who concluded that $Ri' = 1.4$ is still applicable to explain the plug-holing and boundary layer separation phenomena associated with smoke boundary layers. Zhang et al. [22] further studied the influence of the shaft size on the plug-holing height which indicates the degree of smoke layer plug-holing, and built a model for predicting the critical shaft height through a series of numerical tunnel fire simulations. However, Zhao et al. [23] gave a new dimensionless Ri^* by finding that Ji's plug-holing criterion [19] could not be applied to large cross-section shafts, and then proposing a prediction model for the plug-holing height based on tunnel fire simulated data. As can be seen, Ri' or Ri^* can describe the smoke flow pattern within tunnel shafts, and its critical value can predict the occurrence of the smoke layer plug-holing. However, the above studies are carried out at standard atmospheric pressure (101 kPa), and then the critical Ri' criterion and the plug-holing height model may not be applicable to the tunnel fires at reduced pressure owing to the various smoke movement patterns at reduced pressure.

Ji et al. [24] carried out a series of simulations in full-scale highway tunnels to explore the effect of ambient pressure on the temperature distribution in tunnel fires, and the results showed that the longitudinal temperature distribution increased with the decrease of ambient pressure. Tang et al. [25] found that longitudinal smoke temperature decays faster at reduced pressure through numerical simulations. Feng et al. [26] and Liu et al. [27] found that the CO concentration and smoke movement speed in high altitude tunnel fires were different from those standard atmospheric pressure, and the smoke movement speed increased with the increase in altitude. Wang et al. [28–34] investigated the influence of reduced pressure on the ceiling temperature profile, CO concentration profile and flame height

by full-scale aircraft cargo compartment fire tests to derive prediction models of these fire plume characteristics applicable at reduced pressure. Obviously, the decrease of ambient pressure can change the tunnel fire smoke transportation characteristics, which have a significant impact on the smoke movement pattern during natural smoke extraction from the shaft and the crucial plug-holing criteria values. For this aspect, Yan et al. [35] calculated the critical plug-holing criterion Ri' at 60 kPa, 80 kPa, and 100 kPa and found that Ri' decreased at reduced pressure. However, the mathematical relationship between the critical plug-holing criterion and reduced pressure is not clarified. Moreover, the plug-holing height reflecting the degree of smoke layer plug-holing at reduced pressure has rarely been addressed in previous studies.

Therefore, this work conducted theoretical analysis and numerical simulations to clarify the reduced pressure effects on smoke temperature and velocity in a natural ventilated tunnel with a vertical shaft to present the critical plug-holing criteria and plug-holing height. A new plug-holing criterion and a new prediction model for plug-holing height of tunnel fires with a natural ventilated vertical shaft are proposed to extend the application range of the criterion and prediction model including the standard atmospheric pressure and reduced pressure.

2. Theoretical Analysis

2.1. Plug-Holing Criterion for Vertical Shafts at Reduced Pressure

Ji et al. [19], based on the analysis of the main driving dynamics in the natural smoke exhaust process of the shaft, proposed the dimensionless Ri' number to determine the flow field structure in the shaft, which is defined as the ratio of the vertical thermal buoyancy (F_v) to the horizontal inertial force (F_h) of the smoke, i.e.

$$Ri' = \frac{F_v}{F_h} = \frac{\Delta\rho gh A_{shaft}}{\rho_{s0} v^2 d w_s} \quad (1)$$

where $\Delta\rho$ is density difference between smoke and ambient air without smoke exhaust, g is the gravitational acceleration, h is the shaft height, A_{shaft} is the vertical shaft cross-sectional area, ρ_{s0} is the density of smoke without smoke exhaust, v is the horizontal flow rate of the smoke below the shaft without smoke exhaust, d is the smoke layer thickness below the shaft without smoke exhaust, and w_s is the shaft width.

If the ambient pressure changes, $\Delta\rho$ and ρ_{s0} will change as well. According to the ideal gas law:

$$PV = nRT \quad (2)$$

where P is the pressure of ideal gas, V is the volume of ideal gas, n is the amount of gas substance, R is the ideal gas constants, and T is the thermodynamic temperature of ideal gas. It can be obtained from the ideal gas equation:

$$p \propto \rho T \quad (3)$$

where ρ is the smoke density. The density difference between smoke and ambient air can be estimated by [36]:

$$\Delta\rho = \frac{\Delta T_s}{T_s} \rho_{air} = \frac{\Delta T_s}{T_a + \Delta T_s} \rho_{air} \quad (4)$$

where T_s and ΔT_s are the smoke temperature and the smoke temperature rising below the shaft, T_a is the ambient temperature, ρ_{air} is the air density.

He [37] proposed an empirical equation for predicting the velocity of smoke below the ceiling based on experimental results and theoretical analysis of narrow and long space fires, ie.

$$v = 0.8 \left(\frac{g Q_c T_s}{2 C_p \rho_{air} T_a^2 w} \right)^{1/3} \quad (5)$$

where Q_c is the convective heat release rate, C_p is the specific heat of air, and w is the width of the tunnel.

The heat release rate can be expressed as [38]:

$$Q_c = \dot{m} h_c \quad (6)$$

where \dot{m} is burning rates and h_c is the heat of combustion.

Wieser et al. [39] obtained the average burning rate of n-heptane fire is approximately proportional to the 1.3 power of atmospheric pressure:

$$\dot{m} \propto p^{1.3} \quad (7)$$

where p is the ambient pressure.

Combining Eqs. (6) and (7), the relationship between the heat release rate and pressure can be expressed as:

$$Q_c \propto p^{1.3} \quad (8)$$

Then, the velocity of smoke under the same heat release rate and reduced pressure can be expressed as (ignoring the influence of pressure on the gravitational acceleration):

$$v \propto \left(\frac{Q_c T_s}{\rho_{air}} \right)^{\frac{1}{3}} \quad (9)$$

The smoke temperature T_s can be expressed as:

$$T_s = T_a + \Delta T_s \quad (10)$$

Yin et al. [40] obtained the relationship between plume temperature and pressure through high-altitude combustion chamber experiments, which can be expressed as:

$$\frac{\Delta T_s}{T_0} \sim \left(\frac{P}{Q_c}\right)^{-2/3} \quad (11)$$

Gong et al. [41] pointed out that the longitudinal temperature distribution of the tunnel can be expressed as:

$$\frac{\Delta T_s}{T_a} = A_1 \exp\left(-\frac{x/w}{A_3}\right) + A_2 \exp\left(-\frac{x/w}{A_4}\right) \quad (12)$$

where A_1, A_2, A_3 and A_4 are just fitting coefficients, and x is the longitudinal position from the fire source.

Finally, Yan et al. [35] have pointed out that the influence of pressure on the smoke layer thickness is very small, so ignoring the influence of pressure on the smoke layer thickness. Combining the Eqs. (1), (3), (4), (5), and (9), the expression of Ri'_x under the same heat release rate at reduced pressure can be expressed as:

$$Ri'_x = \left[k_1 \left(\frac{P_x}{p_{std}}\right)^{-0.3} + k_2 \left(\frac{P_x}{p_{std}}\right)^{-0.1} \right]^{-\frac{2}{3}} Ri' \quad (13)$$

where k_1, k_2 are just fitting coefficients, p_{std} and p_x are the standard atmospheric pressure and reduced pressure of x kPa.

2.2. Plug-Holing Height at Reduced Pressure

According to previous studies [23], the plug-holing height is related to Ri' and shaft shape. In order to reveal the quantitative relationship between ambient pressure and plug-holing height, the concepts of pressure coefficient and dimensionless shaft height are introduced here. The pressure coefficient is defined as the ratio of ambient pressure to standard atmospheric pressure:

$$\alpha = \frac{P_x}{p_{std}} \quad (14)$$

The plug-holing height is more sensitive to the shaft opening length [22], and the dimensionless shaft height (h^*) is defined as the ratio of the shaft length to the shaft height as follows.

$$h^* = \frac{l_{shaft}}{h_{shaft}} \quad (15)$$

where l_{shaft} is the shaft length and h_{shaft} is the shaft height.

The dimensionless heat release rate can be calculated as follows [42].

$$Q^* = \frac{Q_c}{\rho_{air} T_a C_p g^{1/2} H^{5/2}} \tag{16}$$

where H is the hydraulic tunnel height defined as the ratio of 4 times the tunnel cross-sectional area to the tunnel perimeter.

Therefore, the dimensionless plug-holing height can be expressed as:

$$h_p^* = \frac{h_p}{h_{shaft}} = f(Ri', h^*, Q^*, \alpha) = k_3 Ri'^{k_4} h^{*k_5} Q^{*k_6} \alpha^{k_7} \tag{17}$$

where h_p is the plug-holing height. k_3, k_4, k_5, k_6 and k_7 are the fitting coefficients. α is the pressure coefficient. h^* is the dimensionless shaft height.

3. Numerical Modeling and Setting

3.1. Fire Scene

A natural ventilated tunnel of 120 m (length) 9 m (width) 6 m (height) with a vertical shaft model is established by FDS 6.6, as shown in Fig. 1. The shaft is located at the longitudinal centerline of the tunnel and 57.5 m from the left tunnel opening. The shaft cross-sectional size is 9 m², 3 m length (l) and 3 m width (w), and the shaft height is adjustable in the range of 0–5 m. For comparison, a fire scenario with no shaft is set up to evaluate the original horizontal inertia force of the smoke. In order to obtain the best simulation result, additional extension areas denoted by yellow are added to the model in Fig. 1.

The ambient pressures are set to 60 kPa, 70 kPa, 80 kPa, 90 kPa, and 101 kPa, which is sufficient to cover the ambient pressure variation characteristics from 0 to 4500 m in altitude [43]. N-Heptane fire sources of 2 m (length) 2 m (width) are located at the longitudinal centerline of the tunnel floor, 37.5 m away from the left tunnel opening. The heat release rates are 3 MW and 10 MW to represent the most common car fires (3 MW) and truck fires (10 MW) in the tunnel. The initial ambient temperature of the tunnel is 20 °C and the duration of the numerical simulation is 1200 s to form the steady state of the smoke movement in the tunnel and the shaft. The fire simulation conditions are summarized in Table 1.

Temperature and velocity vector slices are located at the longitudinal centerline of the shaft to visualize the smoke temperature distribution and flow field. In addition, a series of vertical temperature and velocity measurement points are set up below the shaft opening to get the vertical thermal buoyancy and horizontal inertia forces of the smoke layer below the shaft. The detailed arrangement of measurement points in the model is shown in Fig. 2.

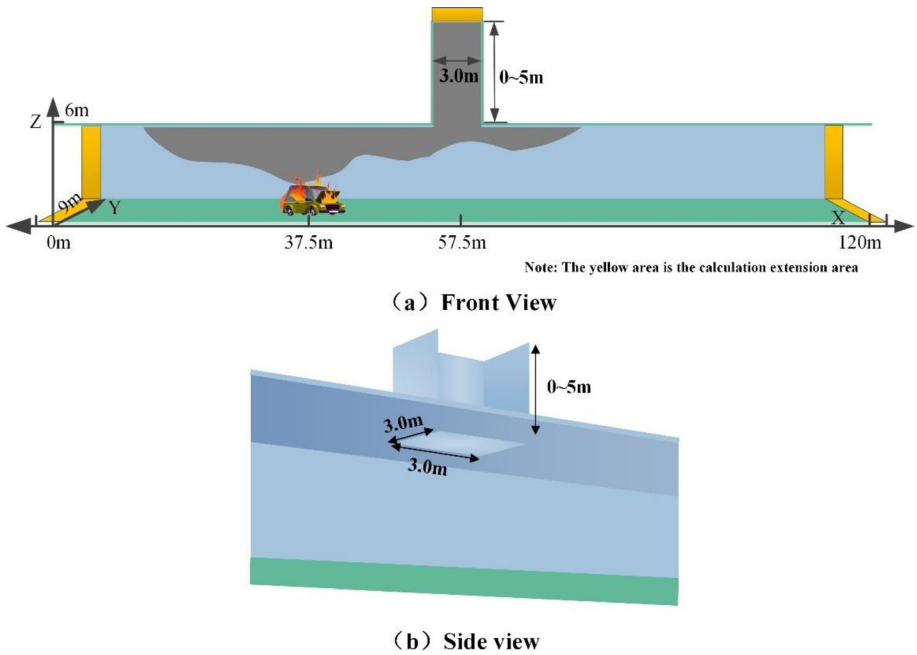


Figure 1. Schematic diagram of the FDS model tunnel.

**Table 1
Fire Condition Setting**

Scenario	Shaft height (m)	Ambient pressure (kPa)	HRR(MW)
1-10	–	60, 70, 80, 90, 101	3, 10
11-20	0.5		
21-30	1		
31-40	1.5		
41-50	2		
51-60	2.5		
61-70	3		
71-80	3.5		
81-90	4		
91-100	5		

3.2. Mesh Analysis

The grid size has an important influence on the accuracy of simulation and calculation time. According to the FDS User’s Guide, when the grid size (d_g) follows: $d_g = 1/16D^* \sim 1/4D^*$, the FDS model has high simulation accuracy [44]. The characteristic diameter D^* can be expressed as follows:

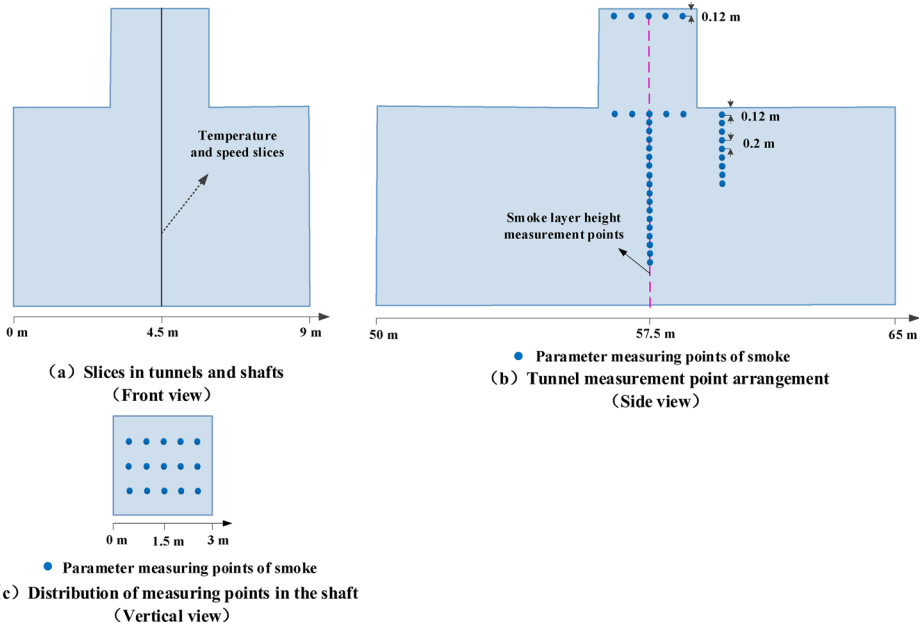


Figure 2. Setting of measurement points in tunnels and shafts.

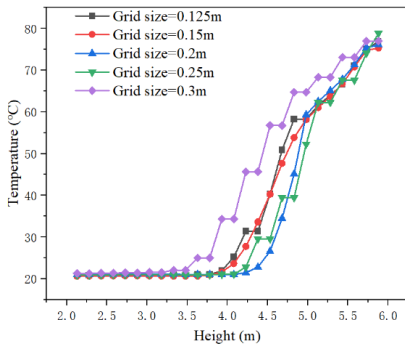
$$D^* = \left(\frac{Q_c}{\rho_{air} C_p T_a \sqrt{g}} \right)^{2/5} \tag{18}$$

According to the ideal gas equation, $\rho_{air} = PM/RT_a$, then Eq. (18) can be changed to:

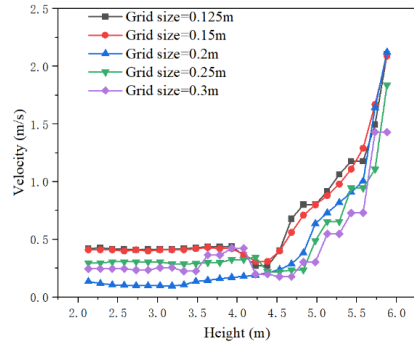
$$D^* = \left(\frac{Q_c R}{P M C_p \sqrt{g}} \right)^{2/5} \tag{19}$$

where M is molar mass of air.

It can be seen from Eq. (19) that the characteristic diameter increases with the increase of HRR and decreases with the increase of pressure. Therefore, the grid independence study is conducted under the conditions of minimum HRR (3 MW) and maximum ambient pressure (101 kPa). Figure 3 shows the vertical distribution of temperature and velocity in the tunnel 12 m to the right of the fire source under different grid sizes. Obviously, when the grid size is less than 0.15 m, there is no obvious difference in the temperature curve. Therefore, considering the calculation accuracy and simulation time, this paper selects the grid size of 0.15 m for FDS simulation. The simulation with different fire source and pressure takes the same grid size (0.15 m) in order to ensure the consistency of the simulation accuracy for each group of working conditions.



(a) The vertical temperature distribution at the location of 12 m away from fire source



(b) The vertical velocity distribution at the location of 12 m away from fire source

Figure 3. Velocity and temperature distribution under different grid sizes.

3.3. Model Validation

Considering the numerical simulation accuracy and calculation time, the FDS grid size was selected as 0.15 m 0.15 m 0.15 m. Since most of the simulated conditions in the work are carried out under pressure boundary conditions, the numerical simulation results by FDS at reduced pressure are compared and verified before carrying out the simulations. Yan et al. [45] conducted six full-scaled fire experiments in the Baimang Snow Mountain No. 1 Tunnel, Yunnan Province, where the ambient pressure was approximately 62.63 kPa, the air density was approximately 0.8353 kg/m³, and the ambient temperature was approximately 13.5 °C in the experimental section of the tunnel. The tunnel ambient characteristics are replicated using FDS, and a typical experimental situation with a fire source power of 0.72 MW is simulated. In comparison to the experimental longitudinal temperature distribution, the results of the numerical simulation of the smoke temperature at 0.12 m below the tunnel ceiling are displayed in Fig. 4a. The smoke temperature is selected from the experimental data at the fully developed stage of the fire. The results show that the simulated temperature is in good agreement with the experimental data.

At the same time, the FDS simulation results under standard atmospheric pressure are also verified. Cong et al. [46] conducted a series of experiments in a 1:15 small-scale tunnel. The full-scale tunnel corresponding to the experimental model is almost the same size of the model tunnel constructed in this paper. Enlarge the small-scale model to a full-scale model scale, and compare the numerical simulation results with the experimental results of the small-scale model, as shown in Fig. 4 (b). It can be seen that under the standard atmospheric pressure, the temperature simulation results below the tunnel ceiling are not significantly different from the experimental data.

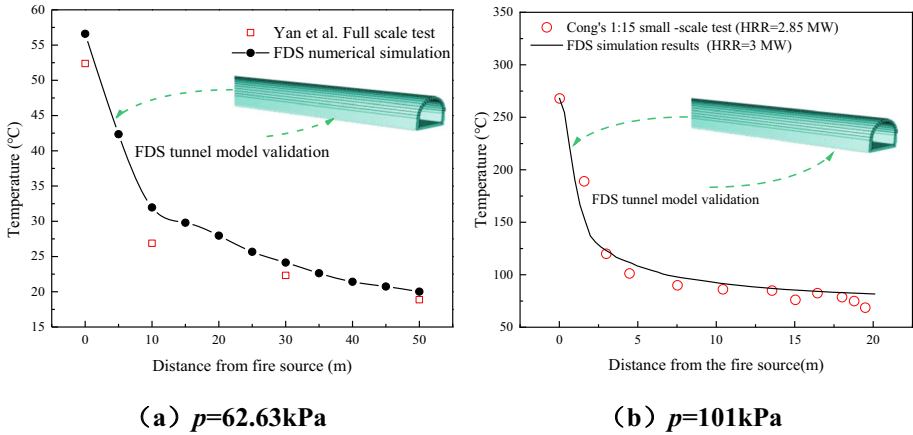


Figure 4. Comparison between simulated and experimental results.

In order to verify the accuracy of the FDS simulation of vertical shaft smoke exhaust, the simulation results were compared with the smoke movement pattern in the 1:6 reduced-size model tunnel by Ji et al. [19]. Ji et al. [19] presented detailed experimental conditions in their study, and the boundary conditions can be well reproduced by FDS. Two representative operating conditions with HRR of 20.21 kW are reproduced in FDS. Figure 5 shows the centerline temperature distribution in the shaft area (left) compared with the experimental results of Ji et al. [19] (right). It can be seen that when the shaft height is 0.2 m, no plug-holing occurs, and when the shaft height is 0.4 m, significant plug-holing has occurred. The two smoke movement patterns are in good agreement when the modeling findings and experimental phenomena are compared side by side. In summary, numerical simulations can satisfy the research needs.

To verify the accuracy of numerical simulation results under other heat release rates, the smoke flow velocity below the tunnel ceiling was compared with previous studies [47]. The comparison between the FDS simulation results and the smoke velocity prediction model Eq. (5) proposed by He [37].

Figure 6 shows the comparison between the smoke flow velocity at a distance of 12 m to the left of the fire source and the predicted results of the Eq. (5). It can be seen that the numerical simulation results are in good agreement with the predicted values of the empirical equation.

In summary, the accuracy of the FDS numerical model is reliable, and it is feasible to simulate fires in high-altitude tunnels under different environmental pressure.

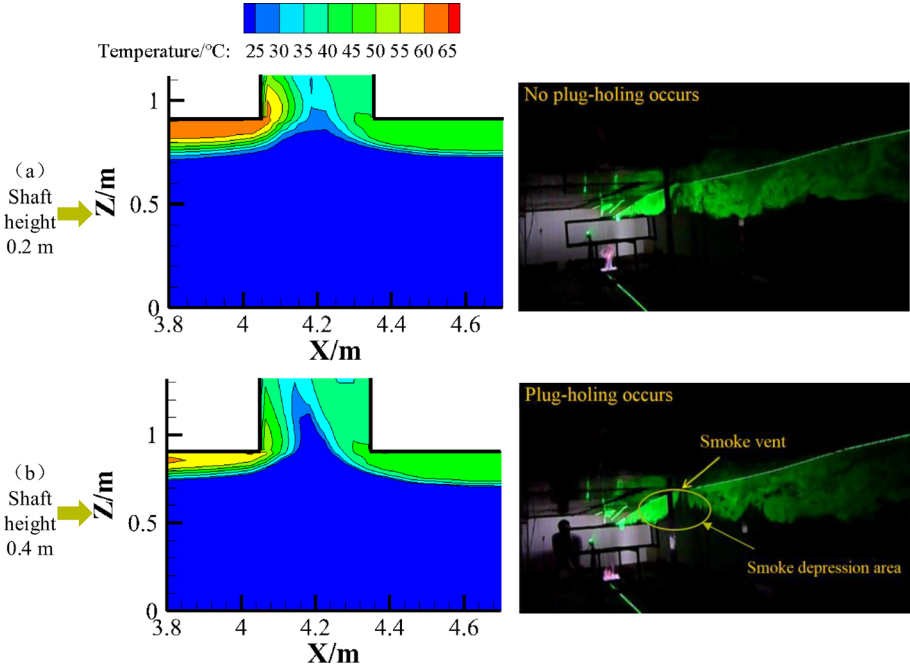


Figure 5. Vertical shaft plug-holing: simulated by FDS (left) and experimental results by Ji et al. [19] (right).

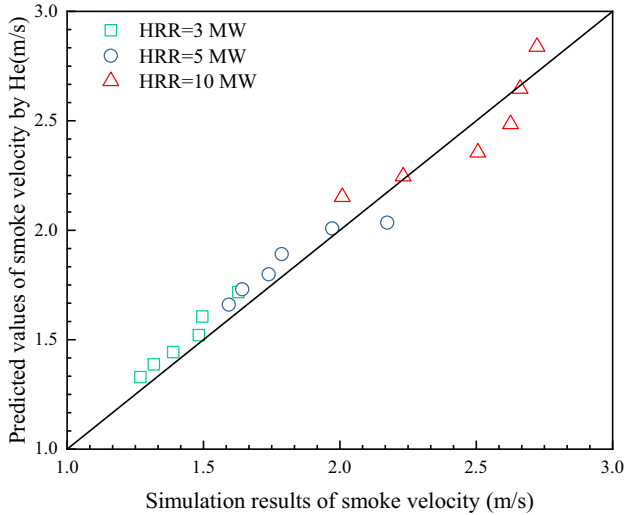


Figure 6. Comparison between simulation results of smoke velocity and predicted values using empirical equation.

4. Results and Discussion

4.1. Smoke Temperature Profile and Velocity Field in the Vertical Shaft

Figure 7 shows smoke temperature distribution at the longitudinal central plane of vertical shafts with different heights at 60 kPa and 101 kPa for 3 MW tunnel fires. When the shaft height is 2 m, the smoke layer below the shaft can still maintain a stable layered structure. However, a low-temperature depression area below the shaft has occurred, where smoke with temperature lower than 40 °C starts to invade the smoke layer at the bottom of the shaft. When the shaft height approaches 2.5 m, smoke with a temperature below 25 °C has obviously descended into the shaft. Since more cold air is sucked into the shaft directly due to the stronger

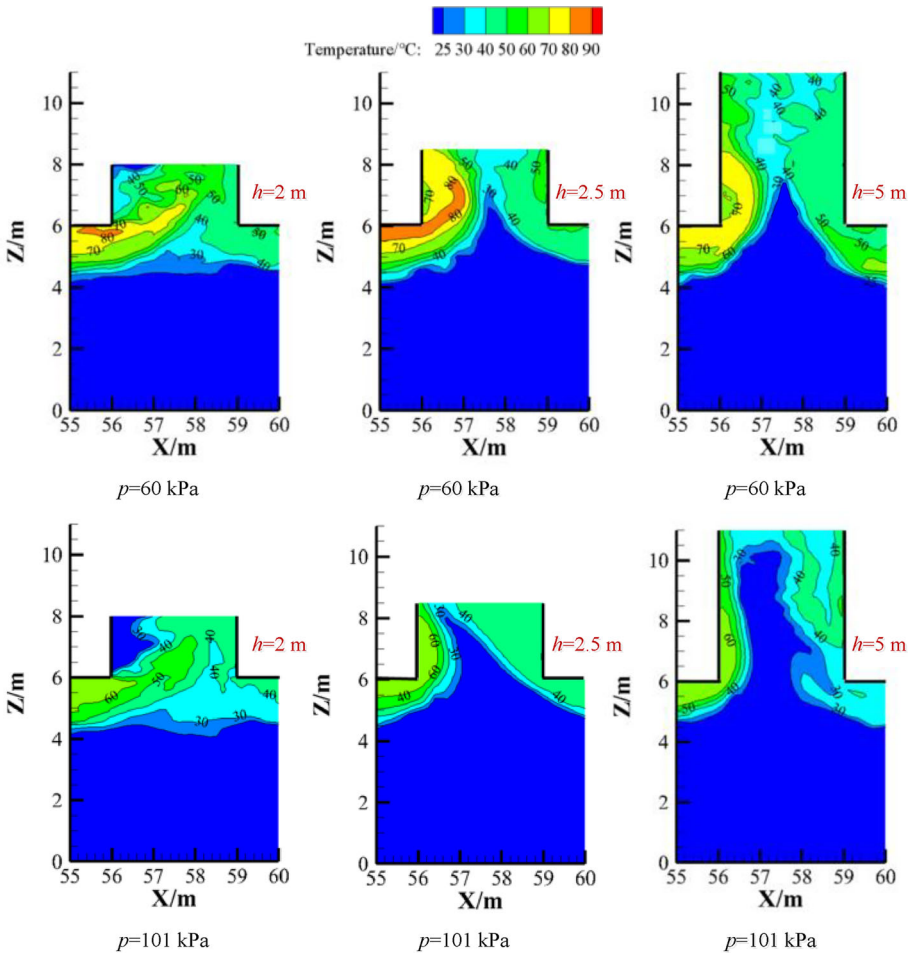


Figure 7. Smoke temperature distribution for different shaft heights at 60 kPa and 101 kPa (HRR= 3 MW).

stack effect of high vertical shaft, the smoke layer thickness beneath the bottom of the shaft decreases to zero, and then smoke layer plug-holing occurs.

With the increase in shaft height, the highest point of the recessed region surpasses the bottom of the shaft and then an obvious cold air cone appears in the shaft. In accordance with the Ri' criteria put forward by Ji et al. [19], smoke layer plug-holing appears in the shaft when the vertical thermal buoyancy causing the stack effect of the smoke is greater than its horizontal inertia force. Thus, for tunnel fires at same pressure, the degree of plug-holing is enhanced by the increasing shaft height, just like the elevating smoke depression point of higher shaft in Fig. 7. Comparing smoke depressed areas for the same shaft height at different pressures, the smoke depression point at 60 kPa is lower than it at 101 kPa, that is, the degree of plug-holing is weakened by the reduced pressure. The quantitative analysis of plug-holing degree and its induced mechanism at reduced pressure is expressed in Sect. 4.3.

The smoke flow velocity field in the shaft can be used to determine the boundary layer separation which means that a vortex area appears on the upstream sidewall of the shaft [48]. Figure 8 shows the smoke flow velocity field in the shaft with different shaft heights at 60 kPa and 101 kPa for 3 MW tunnel fires. When the shaft height is 2 m, a vortex area near the upstream sidewall of the shaft is observed, indicating that boundary layer separation has occurred. And the horizontal inertia force of the smoke is the main driving factor for smoke flow in the shaft, since the stack effect is insufficient to overcome the adverse resistance to smoke exhaust caused by the inverse pressure gradient. The boundary layer separation phenomenon exists when the shaft height is less than 2 m. With the shaft height increasing to 2.5 m, a vortex area near the sidewalls of the shaft disappears and vertical flow vectors appear at the shaft center. Smoke layer plug-holing replaces boundary layer separation and continues to occur for higher shafts, while the stack effect of the shaft is the main driving factor for smoke flow. Clearly, the reduced pressure lengthens the existence of boundary layer separation phenomenon and postpone the occurrence of plug-holing.

According to the smoke temperature and flow velocity field in the shaft, the smoke boundary layer separation and plug-holing phenomena for different shaft heights at different pressures are summarized in Table 2.

4.2. Plug-Holing Criterion at Reduced Pressure

According to the numerical data of smoke temperature rise, smoke layer thickness and smoke velocity listed in Table 3, the critical Ri' at different pressures is calculated using Eq. (1) as shown in Fig. 9. The critical Ri' at standard atmospheric pressure (1.38) agrees with the conclusion reached by Ji et al. [19], and the critical Ri' s at 60 kPa and 80 kPa (1.08 and 1.34 respectively) correspond to Yan's study [35] which further verifies the accuracy of our simulation results further. Obviously, reduced pressure leads to a reduction in the critical Ri' for smoke layer plug-holing. Because the faster smoke flow velocity at reduced pressure caused by a higher smoke temperature as presented in Sect. 4.1, enhances the horizontal inertial force of the smoke layer below the shaft. Figure 10 shows the relationship

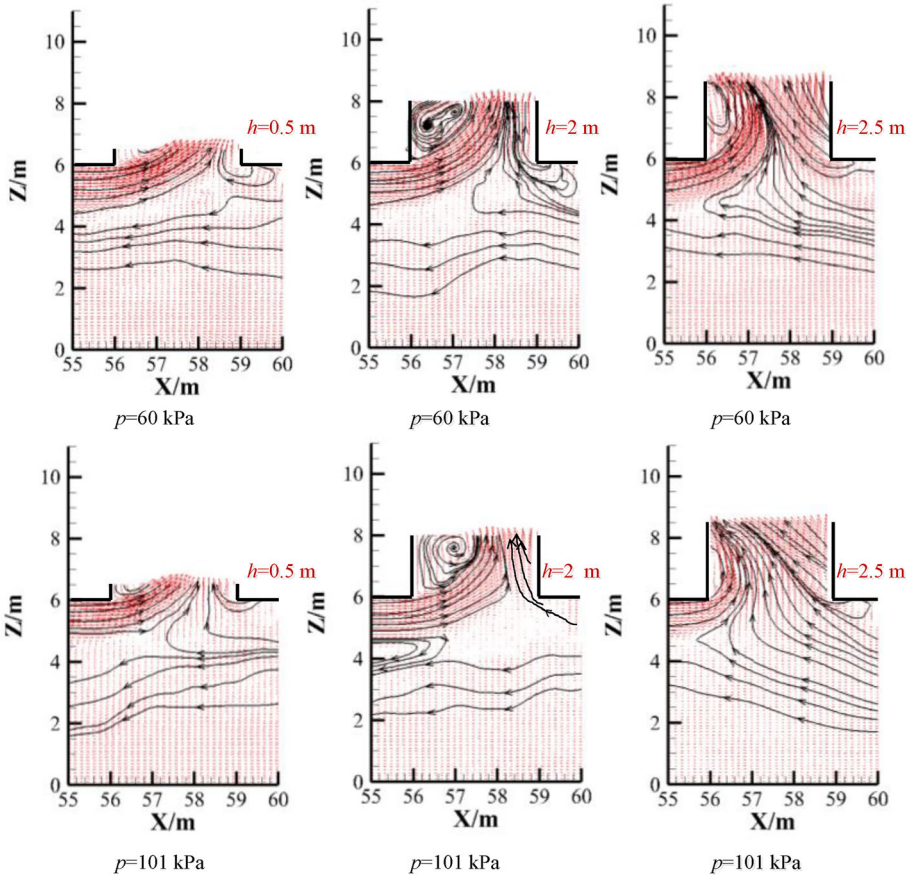


Figure 8. Smoke flow velocity field for different shaft heights at 60 kPa and 101 kPa (HRR=3 MW).

between Ri' and ambient pressure, i.e. the ratio of Ri'_x at reduced pressure to Ri' at standard atmospheric pressure has a non-linear relationship to the pressure coefficient, which corresponds to the theoretical analysis (Eq. 13).

Therefore, the judging criterion of smoke layer plug-holing at reduced pressure Ri'_x can be expressed as Fig. 10.

4.3. Reduced Pressure Effect on Plug-Holing Height

The concept of plug-holing height is proposed to describe the degree of plug-holing, which is defined as the vertical height difference between the bottom opening of the shaft and the highest point of the low-temperature depression zone at 5 °C temperature rise in the shaft, denoted as h_p [23]. Figure 11 gives the plug-holing height at different pressures for 3 MW tunnel fires with 5 m shaft height through smoke temperature fields in the shaft. The plug-holing height decreases by 66%

Table 2
Smoke Boundary Layer Separation and Plug-Holing Phenomena for Different Shaft Heights at Different Pressures

Shaft height (m)	HRR									
	60 kPa		70 kPa		80 kPa		90 kPa		101 kPa	
	3 MW	10 MW	3 MW	10 MW	3 MW	10 MW	3 MW	10 MW	3 MW	10 MW
0.5	B	B	B	B	B	B	B	B	B	B
1	B	B	B	B	B	B	B	B	B	B
1.5	B	B	B	B	B	B	B	B	B	B
2	B	B	B	B	B	B	B	B	B	B
2.5	P	B	P	B	P	B	P	B	P	P
3	P	P	P	P	P	P	P	P	P	P
3.5	P	P	P	P	P	P	P	P	P	P
4	P	P	P	P	P	P	P	P	P	P
4.5	P	P	P	P	P	P	P	P	P	P
5	P	P	P	P	P	P	P	P	P	P

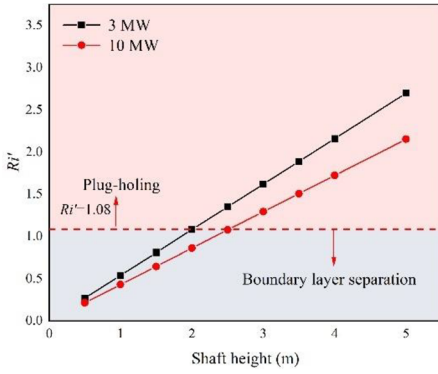
“B” indicates the occurrence of boundary layer separation phenomenon, “P” indicates the occurrence of plug-holing phenomenon

Table 3
Smoke Layer Parameters Below the Shaft Opening

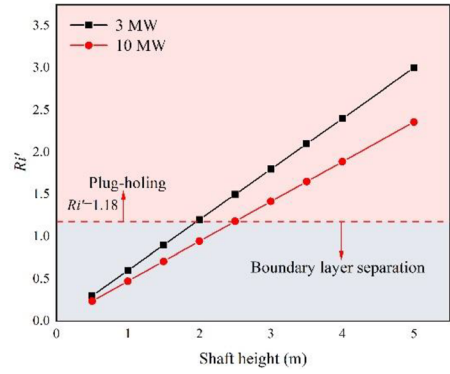
Ambient pressure (kPa)	HRR (MW)	Smoke temperature rising (K)	Smoke layer thickness (m)	Smoke velocity (m/s)
60	3	45.4	1.8	2.2
	10	107.9	1.9	3.6
70	3	43.0	1.8	2.0
	10	103.2	1.8	3.5
80	3	38.9	1.7	1.8
	10	92.5	1.9	3.1
90	3	36.8	1.8	1.8
	10	89.8	1.9	2.9
101	3	35.3	1.8	1.7
	10	81.4	1.9	2.8

when the pressure decreases from standard atmospheric pressure to 60 kPa. Reduced pressure has a non-negligible influence on the plug-holing height.

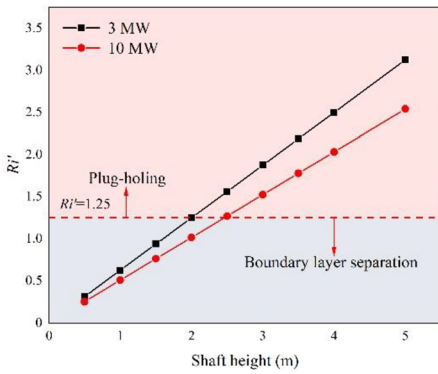
Figure 12 presents all plug-holing heights for tunnel fires of different heat release rates with various shaft heights at different pressures, showing that the plug-holing height decreases with the decrease of the ambient pressure for tunnel fires with the same heat release rate, and the heat release rate decreases the plug-holing height for the same pressure and shaft height condition. In addition, at the same pressure, the plug-holing height shows an overall upward trend with the increase in shaft height, which supports Zhao’s [23] study at standard atmospheric pressure.



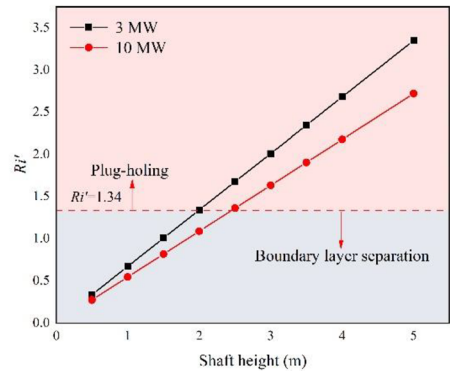
(a) $p=60$ kPa



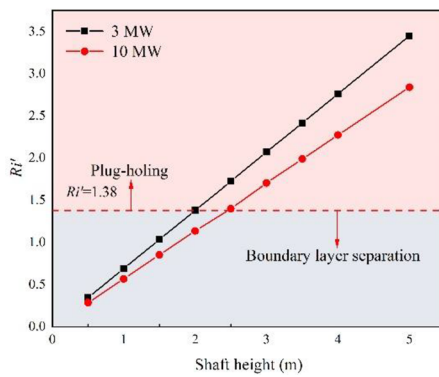
(b) $p=70$ kPa



(c) $p=80$ kPa



(d) $p=90$ kPa



(e) $p=101$ kPa

Figure 9. Ri' values of smoke plug-holing tunnel shaft at different pressures.

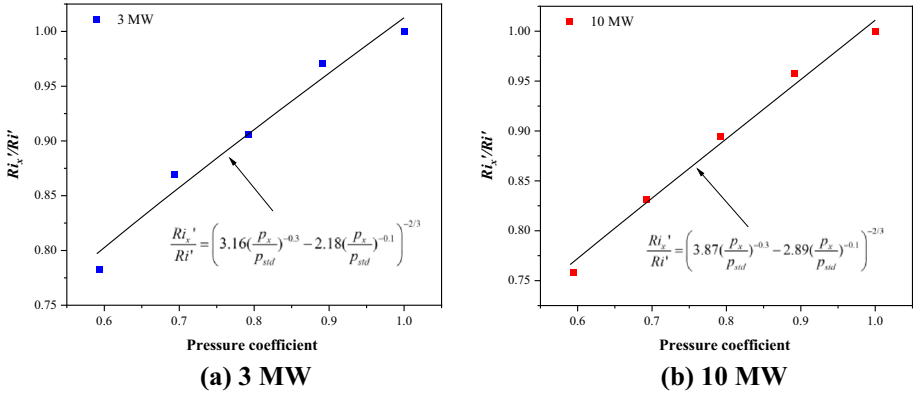


Figure 10. Correlation between Ri_x'/Ri' and ambient pressure coefficient.

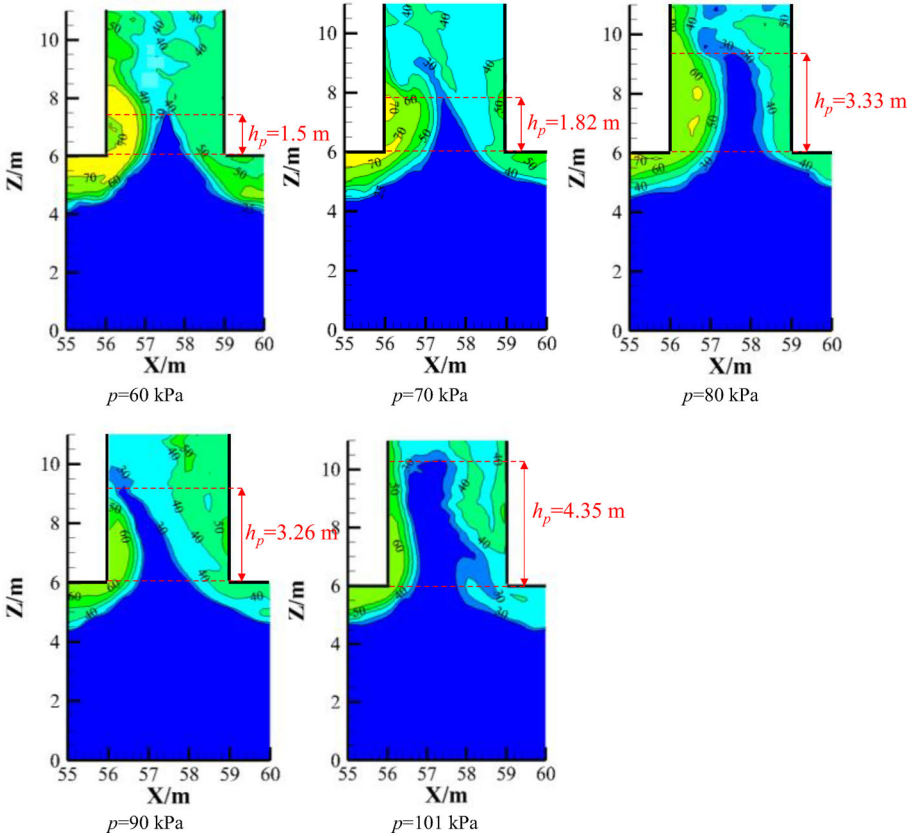


Figure 11. Plug-holing height of the shaft at different pressures (HRR= 3 MW, h = 5 m).

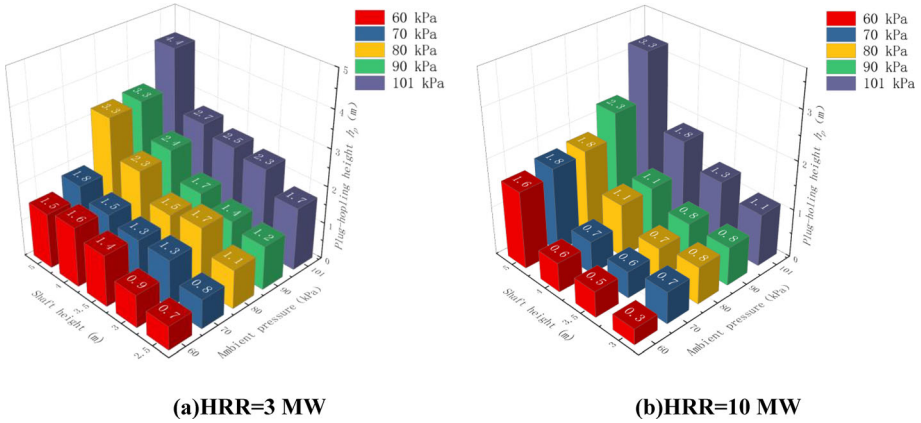


Figure 12. Plug-holing height at different pressures (60, 70, 80, 90, 101 kPa) and shaft heights.

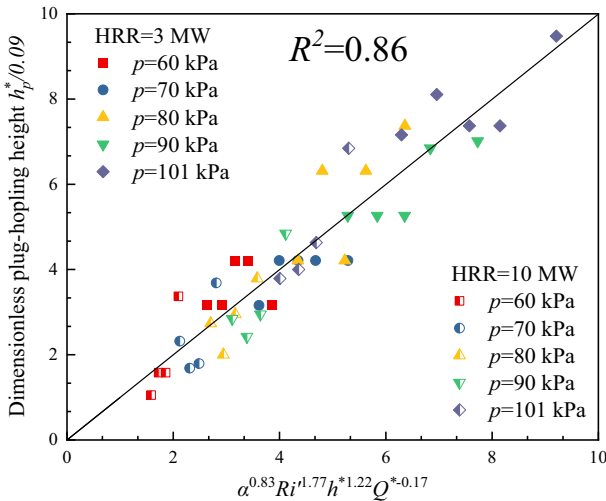


Figure 13. Dimensionless plug-holing height correlation at different pressures.

Through the theoretical analysis in Sect. 2.2, the dimensionless plug-holing height can be expressed by Eq. (17). Based on the critical Ri' values from the numerical results, Fig. 13 gives the correlation of dimensionless plug-holing height by introducing pressure coefficient α , and the dimensionless shaft height h^* , expressed as:

$$h_p^* = 0.09\alpha^{0.83} Ri^{1.77} h^{*1.22} Q^{*-0.17} \tag{20}$$

5. Conclusion

The plug-holing behavior of smoke layer of tunnel fires with natural ventilated vertical shafts at reduced pressure is studied through theoretical analysis and numerical simulations. The impact of reduced pressure on smoke temperature and flow velocity in the vertical shaft is clarified. And the plug-holing criterion for the smoke layer at reduced pressure, together with the critical judging values, are presented. Then the plug-holing heights at reduced pressure are analyzed. The main conclusions include:

- (1) The plug-holing criterion Ri' for tunnel fires with natural ventilated vertical shafts at reduced pressure is given through theoretical analysis, which has a non-linear relationship to the ambient pressure. The critical judging values of Ri' at 60 kPa, 70 kPa, 80 kPa, 90 kPa are calculated as 1.08, 1.18, 1.25, 1.34 respectively to verify that the critical plug-holing criterion decreases with the reduction of the ambient pressure.
- (2) The plug-holing height decreases with the decreasing pressure, that is, the plug-holing degree of the smoke layer in tunnel fires with a vertical shaft is weakened by the reduced pressure. Because the horizontal inertia force of fire smoke is enhanced by the increasing smoke flow velocity and temperature at reduced pressure.
- (3) A global prediction model (Eq. (20)) for the plug-holing height of tunnel fires with a vertical shaft is proposed by introducing a pressure coefficient and extending the engineering application range. The plug-holing height is proportional to the 1.77 power of Ri' , 1.22 power of h^* , the -0.17 power of the Q^* and the 0.83 power of the pressure coefficient.

Acknowledgements

This work was supported by National Natural Science Foundation of China under Grant No. 52076199 and 51806156; Project of Hubei Provincial Department of Education under Grant No. B2021012.

References

1. Guo C, Guo QH, Zhang T, Li W, Zhu HH, Yan ZG (2022) Study on real-time heat release rate inversion for dynamic reconstruction and visualization of tunnel fire scenarios. *Tunnel Undergr Space Technol* 122:104333
2. Wang MN, Guo XH, Yu L, Zhang YT, Tian Y (2021) Experimental and numerical studies on the smoke extraction strategies by longitudinal ventilation with shafts during tunnel fire. *Tunnel Undergr Space Technol* 116:104030
3. Li H, Tang F (2022) Numerical and experimental study on the critical velocity and smoke maximum temperature in the connected area of branch tunnel. *Build Simul Tsinghua Univ Press* 15(4):525–536

4. Li Z, Zhang Y, Jiang H, Tang C, Luo D, Chen L, Lin Y, Li T (2022) Effect of fire source elevation on the smoke spreading characteristics in an extra-long tunnel. *Fire Technol* . [10.1007/s10694-022-01299-y](https://doi.org/10.1007/s10694-022-01299-y)
5. Tang F, He Q, Chen L, Li P (2019) Experimental study on maximum smoke temperature beneath the ceiling induced by carriage fire in a tunnel with ceiling smoke extraction. *Sustain Cities Soc* 44:40–45
6. Ren F, Shi CL, Li J, Che HL, Xu X (2021) Numerical study on the flow characteristics and smoke temperature evolution under double fires condition with a metro train in tunnel. *Tunnel Undergr Space Technol* 114:10443
7. Kashef A, Saber HH, Gao L (2011) Optimization of emergency ventilation strategies in a roadway tunnel. *Fire Technol* 47(4):1019–1046
8. Yi L, Wang XF, Yang Y, Wang YX, Zhou Y (2020) A simplified mathematical model for estimating gas temperature and velocity under natural smoke exhaust in sloping city tunnel fires. *Sustain Cities Soc* 55:102071
9. Ji J, Li KY, Zhong WZ, Huo R (2010) Experimental investigation on influence of smoke venting velocity and vent height on mechanical smoke exhaust efficiency. *J Hazard Mater* 177(1–3):209–215
10. Cano-Moreno JD, de Pedro JMMS, Esteban BS, Nicolau MS (2021) Influence of the slope and delay on passenger evacuation from a fire along a railway tunnel with natural ventilation. *Fire Technol* 57(4):1569–1588
11. Chen J, Long Z, Wang L, Xu BZ, Bai QL, Zhang YB, Liu C, Zhong MH (2022) Fire evacuation strategy analysis in long metro tunnels. *Saf Sci* 147:105603
12. Król A, Król M (2021) Numerical investigation on fire accident and evacuation in a urban tunnel for different traffic conditions. *Tunnel Undergr Space Technol* 109:103751
13. Li Q, Kang J, Wu Y, Luo J (2022) Theoretical and numerical study of smoke back-layering length for an inclined tunnel under longitudinal ventilation. *Fire Technol*. 58(4):2143–66
14. Zhang S, Yang H, Yao Y, Zhu K, Zhou Y, Shi L, Cheng X (2017) Numerical investigation of back-layering length and critical velocity in curved subway tunnels with different turning radius. *Fire Technol* 53(5):1765–1793
15. Zhang TH, Wang GY, Li JD, Huang YD, Zhu K, Wu K (2021) Experimental study of back-layering length and critical velocity in longitudinally ventilated tunnel fire with various rectangular cross-sections. *Fire Saf J* 126:103483
16. Zhao P, Yuan ZY, Yu NY, Liang CC (2020) Effect of heat release rate and exhaust vent settings on the occurrence of plug-holing during tunnel fires with two-point extraction ventilation. *Tunnel Undergr Space Technol* 106:103617
17. Liu YL, Chen JZ, Yang D (2022) Experimental study on the effects of exhaust vent layout on plug-holing for ceiling central smoke extraction in road tunnel fires. *Tunnel Undergr Space Technol* 126:104550
18. Liu Q, Xu Z, Fan C, Tao H, Zhao J, He L (2022) Experimental and numerical study of plug-holing with lateral smoke exhaust in tunnel fires. *Fire Technol* . [10.1007/s10694-022-01241-2](https://doi.org/10.1007/s10694-022-01241-2)
19. Ji J, Gao ZH, Fan CG, Zhong W, Sun JH (2012) A study of the effect of plug-holing and boundary layer separation on natural ventilation with vertical shaft in urban road tunnel fires. *Int J Heat Mass Transfer* 55(21/22):6032–6041
20. Jiang TH, Cong HY, Kong XX, Li GC, Tan Q, Wang XS (2018) Simulation study on the effect of longitudinal ventilation on smoke exhaust from tunnel shafts. *Fire Sci* 27(1):14–22

21. Jiang XP, Xiang Y, Wang ZY, Mao YSY, Park H (2020) A numerical study on the effect of the shaft group arrangement on the natural ventilation performance in tunnel fires. *Tunnel Undergr Space Technol* 103:103464
22. Zhang SG, He K, Yao YZ, Peng M, Yang H, Wang JH, Cheng XD (2018) Investigation on the critical shaft height of plug-holing in the natural ventilated tunnel fire. *Int J Therm Sci* 132:517–533
23. Zhao SZ, Xu L, Obadi I, Wang F, Liu F, Weng MC (2021) Plug-holing height and complete plug-holing phenomenon in naturally ventilated tunnel fires with vertical shaft. *Tunnel Undergr Space Technol* 107:103631
24. Ji J, Guo F, Gao ZH, Zhu JP, Sun JH (2017) Numerical investigation on the effect of ambient pressure on smoke movement and temperature distribution in tunnel fires. *Appl Therm Eng* 118:663–669
25. Tang F, Hu LH, Yang LZ, Qiu ZW, Zhang XC (2014) Longitudinal distributions of CO concentration and temperature in buoyant tunnel fire smoke flow in a reduced pressure atmosphere with lower air entrainment at high altitude. *Int J Heat Mass Tran* 75:130–134
26. Feng X, Jiang Z, Zhang GL, Luo X, Zeng FB (2022) Study on CO diffusion law and concentration distribution function under ventilation after blasting in high-altitude tunnel. *J Wind Eng Ind Aerod* 220:104871
27. Liu B, Mao J, Xi YH, Hu JW (2021) Effects of altitude on smoke movement velocity and longitudinal temperature distribution in tunnel fires. *Tunn Undergr Sp Technol* 112(4):103850
28. Wang J, Cui GYS, Kong XW, Lu KH, Jiang XP (2022) Flame height and axial plume temperature profile of bounded fires in aircraft cargo compartment with low-pressure. *Case Stud Therm Eng* 33:101918
29. Wang J, Cui G Y S, Lu K H, Jiang X P (2022) Reduced pressure effect on the center-line plume temperatures of elevated N-Heptane fires in an aircraft cargo compartment. *Combust Sci Technol*: 1–17
30. Wang J, Cui GYS, Lu KH, Jiang XP (2021) Reduced pressure effect on the flame length of elevated N-Heptane fires in an aircraft cargo compartment. *Combust Sci Technol* 194(13):2641–2658
31. Wang J, Pan YY, Lu KH, Chen WS, Zhang HJ (2017) Investigation on the CO concentration decay profile and spread velocity of a ceiling jet at reduced pressure in aircraft cargo compartment fires. *Appl Therm Eng* 127:1246–1251
32. Wang J, Lu KH, Lu S, Zhang HJ (2017) Experimental study on ceiling temperature profile of sidewall fires at reduced pressure in an aircraft cargo compartment. *Exp Therm Fluid Sci* 82:326–332
33. Wang J, Lu S, Guan Y, Lo XM, Zhang HP (2015) Experiment investigation on the influence of low pressure on ceiling temperature profile in aircraft cargo compartment fires. *Appl Therm Eng* 89:526–533
34. Wang J, Pan YY, Lu S, Lu KH, Chen WS (2017) CO concentration decay profile and ceiling jet entrainment in aircraft cargo compartment fires at reduced pressures. *Appl Therm Eng* 110:772–778
35. Yan G, Wang M, Yu L, Duan R, Xia P (2020) Effects of ambient pressure on smoke movement patterns in vertical shafts in tunnel fires with natural ventilation systems. *Build Simul* 13(4):931–941
36. Guo F, Gao Z, Wan H, Ji J, Yu L, Ding L (2019) Influence of ambient pressure on critical ventilation velocity and backlayering distance of thermal driven smoke in tunnels with longitudinal ventilation. *Int J Therm Sci* 145:105989

37. He Y (1999) Smoke temperature and velocity decays along corridors. *Fire Saf J* 33 (1):71–74
38. Li J, Prétrel H, Beji T, Merci B (2021) Influence of fire heat release rate (HRR) evolutions on fire-induced pressure variations in air-tight compartments. *Fire Saf J* 126:103450
39. Wieser D, Jauch P, Willi U (1997) The influence of high altitude on fire detector test fires. *Fire Saf J* 29(2-3):195–204
40. Yin JS, Yao W, Liu QY, Zhou ZH, Wu N, Zhang H, Lin C, Wu T, Meier OC (2013) Experimental study of n-Heptane pool fire behavior in an altitude chamber. *Int J Heat Mass Tran* 62:543–552
41. Gong L, Jiang L, Li SY, Shen N, Zhang YC, Sun JH (2016) Theoretical and experimental study on longitudinal smoke temperature distribution in tunnel fires. *Int J Therm Sci* 102:319–328
42. Xu Z, Zhou D, Tao H, Zhang X, Hu W (2022) Investigation of critical velocity in curved tunnel under the effects of different fire locations and turning radiuses. *Tunn Undergr Sp Technol* 126:104553
43. Yan T (2016) Research on key technology of ventilation in high-altitude single-cavern two-way extra-long highway tunnel. Southwest Jiaotong University, Chengdu
44. McGrattan K, Hostikka S, McDermott R, Floyd J, Weinschenk C, Overholt K (2013) Fire dynamics simulator technical reference guide volume 1: mathematical model. NIST Spec Publ 1018(1):175
45. Yan Z, Guo Q, Zhu H (2017) Full-scale experiments on fire characteristics of road tunnel at high altitude. *Tunn Undergr Sp Technol* 66:134–146
46. Cong HY, Wang XS, Zhu P, Jiang TH, Shi XJ (2017) Improvement in smoke extraction efficiency by natural ventilation through a board-coupled shaft during tunnel fires. *Appl Therm Eng* 118:127–137
47. Ji J, Guo FY, Gao ZH, Zhu JP (2018) Effects of ambient pressure on transport characteristics of thermal-driven smoke flow in a tunnel. *Int J Therm Sci* 125:210–217
48. Fan CG (2015) Research on the development characteristics of tunnel fires and natural smoke extraction methods of shafts. University of Science and Technology of China, Hefei

Publisher's Note Springer Nature remains neutral with regard to jurisdictional claims in published maps and institutional affiliations.

Springer Nature or its licensor (e.g. a society or other partner) holds exclusive rights to this article under a publishing agreement with the author(s) or other rightsholder(s); author self-archiving of the accepted manuscript version of this article is solely governed by the terms of such publishing agreement and applicable law.